CHEMICAL ENGINEERING TRANSACTIONS
VOL. 73, 2019
A publication of AIDIC
The Italian Association of Chemical Engineering
Online at www.aidic.it/cet
Guest Editors: Andrea D'Anna, Paolo Ciambelli, Carmelo Sunseri

ISBN 978-88-95608-70-9; **ISSN** 2283-9216
DOI: 10.3303/CET1973006

Nanoparticles Synthesis in Wet-Operating Stirred Media: Preliminary Investigation with DEM Simulations

Marco Vocciante[a,*], Marco Trofa[b], Gaetano D'Avino[b], Andrea Pietro Reverberi[a]

[a]DCCI, Dipartimento di Chimica e Chimica Industriale, Università degli Studi di Genova, Via Dodecaneso 31, 16146 Genova, Italy.
[b]DICMaPI, Dipartimento di Ingegneria Chimica, dei Materiali e della Produzione Industriale, Università di Napoli Federico II, P.le Tecchio 80, 80125, Napoli, Italy.
marco.vocciante@gmail.com

The growing demand of nanomaterials is pushing towards the development of alternative strategies for the safe and sustainable production of nanoparticles. At the same time, to ensure high performances, a fine control over the product specifications is required.
We focused on a bottom-up method combined with a mechanical disaggregation technique using a wet bead-stirring process, since it provides numerous advantages over other approaches, including the minimization of the nanoparticles air dispersion and a greater control over the final product. However, given the broad variability of the parameters involved in both the setup and operation of the process, it is essential to combine the experiments with a theoretical-simulative study to optimize the design.
The present activity consists in the preliminary simulation of the interactions among the grinding beads, modelled through the discrete element method (DEM), and the magnetic stirrer. This approach, providing information regarding the frequency and energy of collisions, which can be related to the properties of the produced nanoparticles, allows a fine tuning of the process parameters.

1. Introduction

The production of nanoparticles (NPs) and nanostructured materials has had an impressive development in recent years, thanks to their versatility in a wide variety of technical applications. Some examples include their use as drug carriers in cancer therapy (Sun et al., 2014), the manufacture of nanocapsules for biomedical applications (Pastorino et al., 2016), the production of catalysts with improved selectivity and conversion (Fabiano et al., 2015), in particular of high performance photocatalysts for the abatement of numerous pollutants (Reverberi et al., 2018a) and hydrogen recovery (Reverberi et al., 2016), and many other industrial unit operations, such as adsorption, separation, and filtration (Yu et al., 2017).
What makes NPs so attractive in many areas of chemistry and engineering are their peculiar properties, such as the high surface-to-volume ratio, which greatly differentiate their behaviour from that of the bulk materials they are made of, for instance by increasing their chemical reactivity and catalytic capacity (Wang et al., 2015).
Many different approaches can be adopted in the production of nanomaterials, depending on the specific properties of the element or compound to be synthesized. In general, these refer to two opposite strategies, i.e., bottom-up and top-down: in the first case, NPs are obtained by a progressive aggregation around seeds typically constituted by ions or molecules, while in the second case the synthesis proceeds by disaggregation/reduction of a macroscopic substrate.
So far, the bottom-up approach has attracted much more attention, as it is easier to monitor the NPs size during growth than during disaggregation (Reverberi et al., 2018b). Methods of this type are cheap and easily accessible, but they lack in terms of precise control of shape, size, and dispersion of the particles. However, these are crucial factors in many applications. Top-down methods (e.g., lithographic methods) offer advantages in these terms, but they generally suffer from high costs and limited access to the equipment needed for manufacturing (Fu et al., 2018).

Paper Received: 04 April 2018; Revised: 15 September 2018; Accepted: 19 December 2018

Please cite this article as: Vocciante M., Trofa M., D'Avino G., Reverberi A., 2019, Nanoparticles Synthesis in Wet-operating Stirred Media: Preliminary Investigation with Dem Simulations , Chemical Engineering Transactions, 73, 31-36 DOI:10.3303/CET1973006

Despite considerable progress in this field, some major challenges, such as the finding of a technical solution to obtain homogeneous NPs (with reduced size distribution) with a process that is not only simple, but also eco-friendly and economically sustainable, have yet to be overcome (Alnarabiji et al., 2017).
One must also take into account that, when a chemical process is adopted for the synthesis of NPs, various chemicals are used as reagents, complexing agents, and surfactants: these substances can be toxic, irritant, mutagens or otherwise harmful to humans or the environment. As a consequence, research is now focused on developing new approaches that are economical, inherently safe, and eco-friendly in order to meet more stringent constraints of environmental safeguard (Meramo et al., 2018). Indeed, both the reagent replacement and the adoption of new procedures imply a new trade-off between environmental sustainability, reaction yield and safety conditions linked to changes in the process settings (Reverberi et al., 2017).
In the present study, we consider an innovative 'bottom-up/top-down coupled' experimental approach, in which various NPs (from zerovalent metal elements to metallic and non-metallic compounds) can be safely produced by precipitation/cementing (bottom-up) and subsequent mechanical refinement (top-down) in wet-operating stirred media (Reverberi et al., 2018b).
The use of equipment such as wet mills brings numerous advantages compared to the dry solution: first of all, a minimization of the air dispersion of the NPs, which are produced directly as a dispersed phase in the process solvent, as well as a greater control over the final product, since the presence of the solvent hinders the re-agglomeration of solid particles that instead occurs when working in dry conditions.
Given the high variability of the parameters involved in the setup and use of the equipment (not just the materials composing the NPs, but also the size and nature of the beads and the type of solvents, to name a few), a combination of experiments and a theoretical-simulative study is recommended. This is essential for the optimal design of the process, which depends on the physico-chemical properties of the materials used, and for the prediction of the nanostructural properties of the final product.
A rather rigorous simulative study would imply a complex multi-phase system, to be modelled by coupling a CFD technique for the description of the solvent fluid dynamics and a DEM one for the dynamics of the solid particles (Trofa et al., 2019). Given the particular configuration of the experimental setup (high particle volume fraction and confinement), the system dynamics is mainly governed by particle-particle collisions. Hence, as a good approximation, the present preliminary study will focus on the solid dynamics (DEM) to investigate the main properties of the overall system. In particular, it is possible to trace the movement of the grinding beads and deduce their collision frequency and energy (Beinert et al., 2015), which can be related (by comparison with the experiments) to the properties of the produced NPs, allowing to predict the conditions that optimize the process.

2. Materials and methods

2.1 Experimental set-up

As anticipated, the production of NPs has been conceived as a two-step process that includes a first phase (optional in some cases) in which the substance (element or compound) is prepared, and a second phase in which the formed agglomerates are disaggregated/abraded by means of a wet mill agitation technique, releasing primary nanoparticles.
In this second stage, main object of the present study, the particles agglomerates produced in the first step are dispersed in a suitable solvent (e.g., propylene glycol or ethanol plus various surfactants) and placed in a glass container with a magnetic PTFE coated stirring bar. We use a cylindrical container with hemispherical base and an internal diameter of 13 mm. The cylindrical magnetic bar, with hemispherical ends, has a diameter of 4.6 mm and a length of 15 mm, thus assuming a slanted position inside the container (with an angle of 40 degrees from the horizontal, and the centre located on the container axis, 3 mm above the centre of the hemispherical base).
Forty beads of non-porous zirconia (ZrO_2) with diameter of 3 mm are then added, forming a packed bed up to 5 mm below the meniscus of the solution. Zirconia has been chosen for its high surface hardness and known anti-scratch properties. Experiments have shown that this configuration avoids the magnet to get stuck, whereas such phenomenon can occur by increasing the number of spheres or their dimension.
Four beads of metallic copper of the same dimensions of the grinding beads have been further added in place of the nanoparticle aggregates, to facilitate the investigation of the mechanical refining phase.
The stirring bar rotates around the container axis with a rotational velocity in the range 300-900 rpm, inducing collisions among the particles. Experiments have also shown that higher rotational speed causes the stirring bar to rise up inside the bed (with consequent loss of efficiency).

2.2 Numerical set-up

The computational domain used in our simulations is schematically reported in Figure 1. Here, the triangular meshes representing the container (black) and the stirring bar (red) are only used to check the contacts with the particles. The blue and red beads denote the ZrO_2 and Cu particles, respectively. A Cartesian reference frame is set with the origin in the centre of the container hemispherical base, with the z-axis along the axis of the cylindrical section of the container. The rotation around the container axis is imposed on the bar mesh.

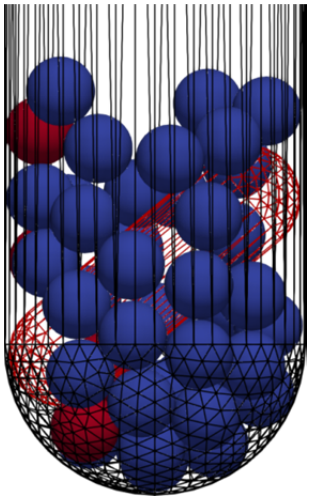

Figure 1: Representation of the simulation domain, with the magnetic bar stirring the beads (blue for ZrO_2 and red for Cu)

The numerical simulations are carried out by adopting the DEM method (Marshall and Li, 2014), which is a Lagrangian model allowing to track the particles by explicitly solving their trajectories. The i-th particle position $\boldsymbol{x}_\mathrm{p}$ and angular position $\boldsymbol{\theta}_\mathrm{p}$ are updated by integrating the following kinematic equations:

$$\frac{d\boldsymbol{x}_\mathrm{p}}{dt} = \boldsymbol{u}_\mathrm{p}, \quad \frac{d\boldsymbol{\theta}_\mathrm{p}}{dt} = \boldsymbol{\omega}_\mathrm{p} \tag{1}$$

where $\boldsymbol{u}_\mathrm{p}$ and $\boldsymbol{\omega}_\mathrm{p}$ are the particle translational and angular velocities. In order to get an initial random particle distribution in systems with high volume fraction, it is common practice in DEM simulations to add the particles in a bigger volume and let them settle. Hence, a cylindrical domain with the same diameter of the container and height 30 mm, placed above the stirring bar at z = 10 mm, has been used. In all the simulations $\boldsymbol{u}_{\mathrm{p},0} = \boldsymbol{\theta}_{\mathrm{p},0} = \boldsymbol{\omega}_{\mathrm{p},0} = \boldsymbol{0}$.
The particle translational and angular velocities are computed from the force and torque balances:

$$m_\mathrm{p}\frac{d\boldsymbol{u}_\mathrm{p}}{dt} = \sum_j \boldsymbol{F}_\mathrm{c} + m_\mathrm{p}\boldsymbol{g}, \quad I_\mathrm{p}\frac{d\boldsymbol{\omega}_\mathrm{p}}{dt} = \sum_j \boldsymbol{T}_\mathrm{c} \tag{2}$$

where m_p and I_p are the particle mass and moment of inertia, $\boldsymbol{F}_\mathrm{c}$ and $\boldsymbol{T}_\mathrm{c}$ are the contact force and torque acting on a given particle due to the other particles or the walls, and $\boldsymbol{g}$ is the gravity force pointing towards the negative z-direction. The contact force and torque are calculated according to the Hertz-Mindlin model (Trofa et al., 2019).
The properties of the materials considered are listed in Table 1 and have been taken from the literature (see Fragnière et al. (2018) for zirconia and glass, Marshall and Li (2014) for copper, and Gondret et al. (2002) for PTFE).

Table 1: Model parameters and material properties

	Zirconia, ZrO_2	Copper, Cu	Glass	PTFE
Density [kg/m^3]	6067	8930	2510	2200
Young's Modulus [GPa]	210.0	120.0	70.0	0.50
Poisson ratio	0.31	0.33	0.24	0.46
Coefficient of restitution	0.92	0.65	0.99	0.80
Coefficient of friction	0.15	0.12	0.27	0.08

To ensure that the contacts of the grinding media are fully resolved and the simulations are stable, a time step of 10^{-7} s has been chosen. This value is lower than 10% of the Rayleigh time and 1% of the Hertz time, i.e., much smaller than the actual contact time of collision, thus fully meeting standard stability criteria (Marshall and Li, 2014).
Typically, the analysed data of a DEM simulation are the number of contacts per unit time, the stress energy distribution and the spatial distribution of the grinding media within the mill. However, the number of contacts at a given time does not correspond to the number of collisions. To calculate the actual number of collisions among particles and walls, a sampling of the contacts at every time step (which is much smaller than the collision time) is required. The impacts and detachments are then obtained by identifying the changes in the contacts; from these, the collision duration can also be computed.
The collision energy is approximated (upper limit) by the kinetic energy based on the relative velocity at the beginning of a contact (Beinert et al., 2015), and is distinguished in normal and tangential direction.
Due to the initialization transient described above, the simulations are run for 0.5 s to let them reach a pseudo steady state condition, then the sampling of the contacts is performed for 0.1 s. To obtain statistical invariance, several simulations with different initial random particle distributions are performed, and the average results considered.
The investigation has been conducted with the open-source software LIGGGHTS® 3.8.0 (more details can be found in Kloss et al. (2012)).

3. Results

In Figure 2 the translational and rotational kinetic energy of all the particles in the system ($ke = 0.5 \sum m_\mathrm{p} u_\mathrm{p}^2$ and $ke_\mathrm{rot} = 0.5 \sum I_\mathrm{p} \omega_\mathrm{p}^2$) are reported for the three stirring velocities considered. The initial overshoot in Figure 2a is due to the initialization procedure, in which the particles are free falling in the container. After about one rotation of the stirrer, a dynamic equilibrium condition with almost constant mean value is achieved. Such mean value is proportional to the rotation velocity, and the fluctuations vary accordingly. The collision frequencies among the particles confirm this trend, with a similar number of impacts in different sampling windows, which is inversely proportional to the rotation velocity. In particular, in the time window 0.5-0.6 s, there are around 12600, 5500, and 3100 collisions for the cases 300, 600, and 900 rpm, respectively.

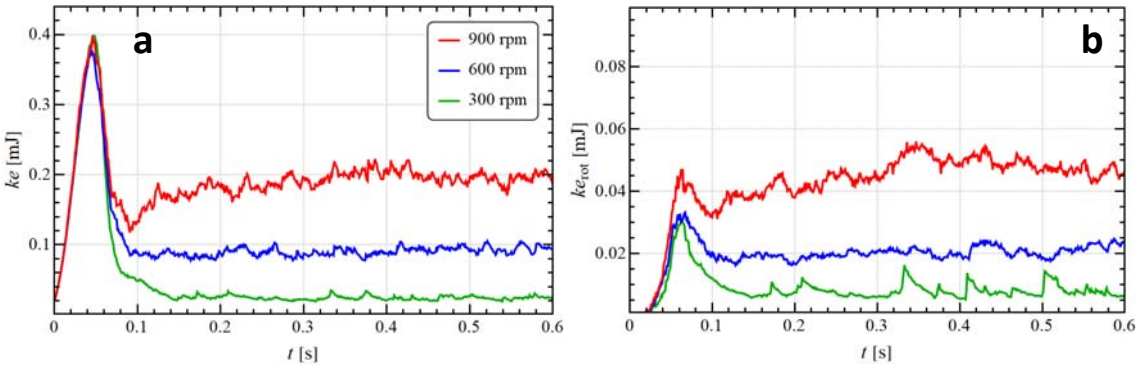

Figure 2: Translational and rotational kinetic energy of all the particles for different stirring velocities

The duration of the collisions and the normal component of the relative velocity at the beginning of a contact ($u_\mathrm{r,n} = \left(\boldsymbol{u}_\mathrm{p,i} - \boldsymbol{u}_\mathrm{p,j}\right) \cdot \boldsymbol{n}$, with $\boldsymbol{n}$ the normal vector to the contact plane) are reported in Figure 3, for all the particles (a-b), and for the collisions involving at least a copper particle (c-d). Data are presented in terms of probability, i.e., the fraction of data corresponding to each bin. This facilitates the comparison among samples of different size, e.g., due to different stirring velocities or type of particles involved. The dashed lines represent the medians of the distributions, which are all unimodal.
Even in the fastest rotation case, the collisions last more than 100 time steps, equivalent to 10 μs (Figure 3a), consistently with the evaluation of the Hertz time, thus ensuring a fine resolution of the contact itself.
By reducing the rotation velocity, the collision time variance increases and the distribution median shifts to higher values, i.e., on average the collisions last longer (Figure 3a). This is connected to a reduction in the velocity particles are moving and colliding with (Figure 3b). Indeed, the same trend can be observed by looking only at the collisions that involve at least a copper particle (Figure 3c-d). Here, also the different particle properties come into play, as the lower Young modulus of the copper particles determines ‘softer’

collisions (lower speed (Figure 3d) and longer duration (Figure 3c)). Since the mechanical properties of the glass are more similar to those of copper than those of zirconia, the duration and normal relative velocity of collisions involving the container walls (not reported) reveal the same behaviour presented in Figure 3c-d.

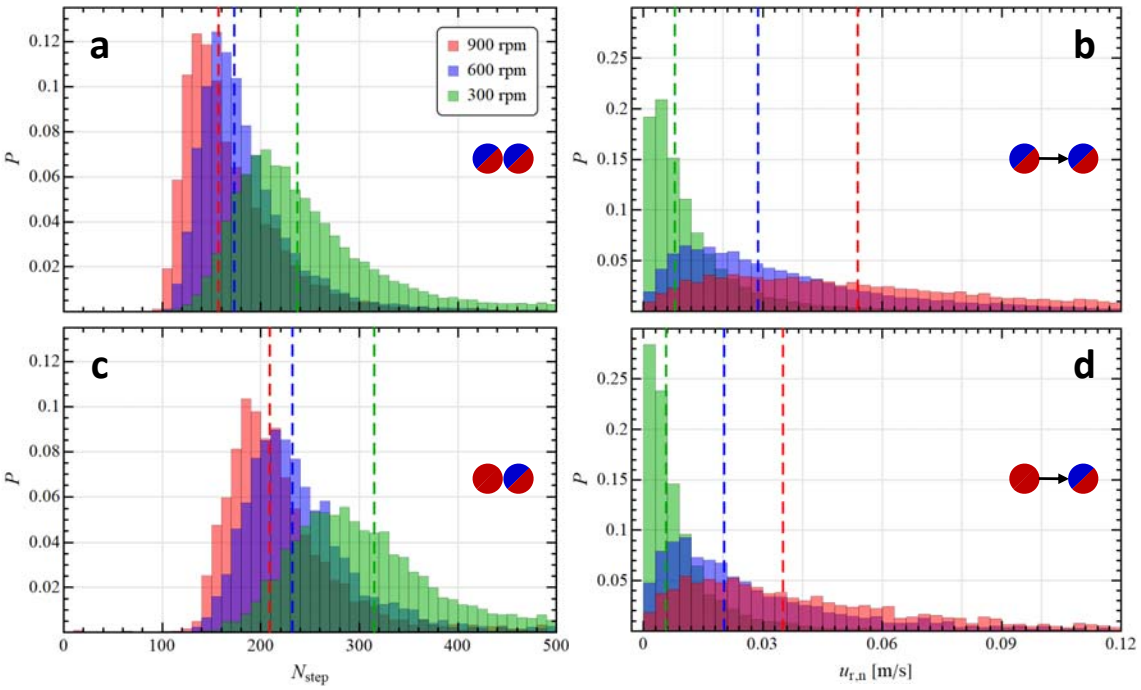

Figure 3: Probability distribution of the contact time and normal relative impact velocity among all the particles (a-b), and for the collisions involving at least a copper particle (c-d), for different stirring velocities

The tangential component of the relative impact velocity ($u_{r,t} = \left\|(\boldsymbol{I} - \boldsymbol{nn}) \cdot (\boldsymbol{u}_{p,i} - \boldsymbol{u}_{p,j}) - r_p(\boldsymbol{\omega}_{p,i} + \boldsymbol{\omega}_{p,j}) \times \boldsymbol{n}\right\|$, with $\boldsymbol{I}$ the identity tensor and r_p the particle radius) for all the particles is reported in Figure 4. The effect of particle material on this quantity is negligible, thus the specific data for copper are not shown. Notice that, while the relative normal collision velocity is about an order of magnitude lower than the bar tip speed (about 0.4 m/s for 600 rpm), the tangential component can be even higher, testifying how the collisions in the rotating system considered are mainly governed by shear. Such consideration is confirmed by the data for the impacts with the container wall, where the particles have the maximum translational velocity and the wall is fixed, resulting in a higher median and variability of the tangential velocity distribution (Figure 4b).

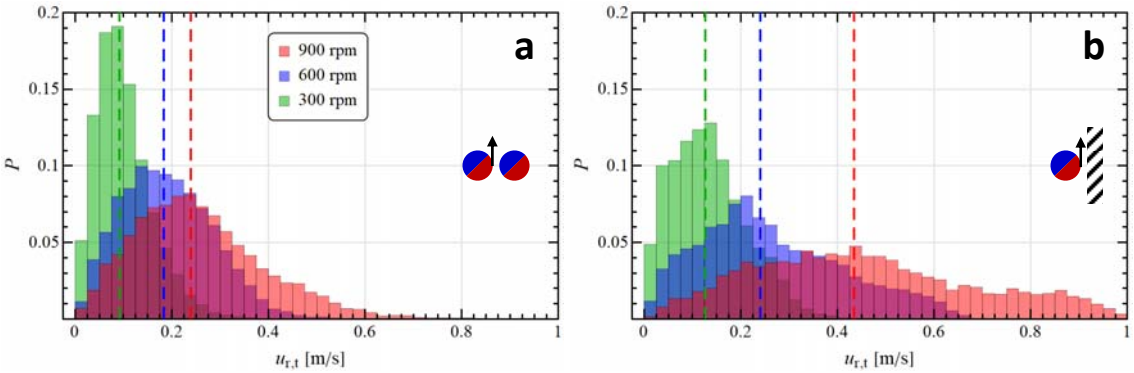

Figure 4: Probability distribution of the tangential relative impact velocity among all the particles (a), and with the container wall (b), for different stirring velocities

4. Conclusions

In this work, a numerical DEM study of wet-operating ball mill stirred with a cylindrical bar has been performed. Three different rotation velocities have been investigated with an in-depth impact analysis to enable a quantification of the actual frequency and the normal/shear components of collisions. The average values from several simulations with different initial random particle distributions have been considered to ensure statistical invariance.

For all the rotation velocities considered, the system has shown a stable dynamics, with a nearly constant impact energy and frequency, the latter resulting inversely proportional to the rotor speed. Furthermore, the collisions have proven to be mainly governed by shear, which is then probably the main responsible for the agglomerate abrasion in a real process.

Indeed, a significant but costly enhancement of the study would consist in the inclusion of the coupled effect between the solid particles and the suspending fluid. Nevertheless, the information here produced about the frequency and energy of contacts, in relation to the process parameters, can already be used for a multi-scale approach (from grinding bead to nanoparticle dynamics), in the development of new nanoparticle production practices that are more economical, inherently safe and eco-friendly.

References

Alnarabiji M.S., Yahya N., Hamed Y., Ardakani S.E.M., Azizi K., Klemes J.J., Abdullah B., Tasfy S.F.H., Hamid S.B.A., Nashed O., 2017, Scalable bio-friendly method for production of homogeneous metal oxide nanoparticles using green bovine skin gelatin, Journal of Cleaner Production 162, 186–194.

Beinert S., Fragnière G., Schilde C., Kwade A., 2015, Analysis and modelling of bead contacts in wet-operating stirred media and planetary ball mills with CFD–DEM simulations, Chemical Engineering Science, 134, 648–662.

Fabiano B., Pistritto F., Reverberi A., Palazzi E., 2015, Ethylene-air mixtures under flowing conditions: a model-based approach to explosion conditions, Clean Technologies and Environmental Policy 17, 1261–1270.

Fragnière G., Beinert S., Overbeck A., Kampen I., Schilde C., Kwade A., 2018, Predicting effects of operating condition variations on breakage rates in stirred media mills, Chemical Engineering Research and Design, 138, 433–443.

Fu X., Cai J., Zhang X., Li W.D., Ge H., Hu, Y., 2018, Top-down fabrication of shape-controlled, monodisperse nanoparticles for biomedical applications, Advanced Drug Delivery Reviews, 132, 169–187.

Gondret P., Lance M., Petit L., 2002, Bouncing motion of spherical particles in fluids, Physics of fluids, 14(2), 643–652.

Kloss C., Goniva C., Hager A., Amberger S., Pirker S., 2012, Models, algorithms and validation for opensource DEM and CFD–DEM, Progress in Computational Fluid Dynamics, an International Journal 12(2-3), 140–152.

Marshall J.S., Li S., 2014, Adhesive particle flow, Cambridge University Press, New York, USA.

Meramo S.I., Bonfante H., De Avila-Montiel G., Herrera-Barros A., Gonzalez-Delgado A., 2018, Environmental assessment of a large-scale production of TiO_2 nanoparticles via green chemistry, Chemical Engineering Transactions, 70, 1063–1068.

Pastorino L., Dellacasa E., Dabiri M.H., Fabiano B., Erokhina S., 2016, Towards the fabrication of polyelectrolyte-based nanocapsules for bio-medical applications, BioNanoScience 6, 496–501.

Reverberi A.P., Klemes J.J., Varbanov P.S., Fabiano B., 2016, A review on hydrogen production from hydrogen sulphide by chemical and photochemical methods, Journal of Cleaner Production 136, 72–80.

Reverberi A.P., Vocciante M., Lunghi E., Pietrelli L., Fabiano B., 2017, New Trends in the Synthesis of Nanoparticles by Green Methods, Chemical Engineering Transactions, 61, 667–672.

Reverberi A.P., Varbanov P.S., Vocciante M., Fabiano B., 2018 a, Bismuth oxide-related photocatalysts in green nanotechnology: A critical analysis, Frontiers of Chemical Science and Engineering, 1–15.

Reverberi A.P., Varbanov P.S., Lauciello S., Salerno M., Fabiano B., 2018 b, An eco-friendly process for zerovalent bismuth nanoparticles synthesis, Journal of Cleaner Production, 198, 37–45.

Sun T., Zhang Y.S., Pang B., Hyun D.C., Yang M., Xia Y., 2014, Engineered nanoparticles for drug delivery in cancer therapy, Angewandte Chemie 53, 12320–12364.

Trofa M., D'Avino G., Sicignano L., Tomaiuolo G., Greco F., Maffettone P.L., Guido S., 2019, CFD-DEM simulations of particulate fouling in microchannels, Chemical Engineering Journal, 358, 91–100.

Wang J., Gu H., 2015, Novel metal nanomaterials and their catalytic applications, Molecules 20, 17070–17092.

Yu L., Ruan S., Xu X., Zou R., Hu J., 2017, One-dimensional nanomaterial assembled macroscopic membranes for water treatment, Nano Today 17, 79–95.